Ceramics International 42 (2016) 11598–11602

Contents lists available at ScienceDirect

Ceramics International

journal homepage: www.elsevier.com/locate/ceramint

# Preparation of a defect-free alumina cutting tool via additive manufacturing based on stereolithography – Optimization of the drying and debinding processes

Maopeng Zhou [a,1], Wei Liu [a,*,1], Haidong Wu [a], Xuan Song [b], Yong Chen [b], Lixia Cheng [a], Fupo He [a], Shixi Chen [a], Shanghua Wu [a,*]

[a] School of Electromechanical Engineering, Guangdong University of Technology, Guangzhou 510006, Guangdong, China
[b] Epstein Department of Industrial and Systems Engineering, University of Southern California, Los Angeles, CA, USA

ARTICLE INFO

*Article history:*
Received 8 March 2016
Received in revised form
8 April 2016
Accepted 11 April 2016
Available online 14 April 2016

*Keywords:*
Stereolithography
Alumina
Drying
Debinding

ABSTRACT

A dense defect-free alumina cutting tool was fabricated via stereolithography process. Different drying processes and debinding profiles were then tested and compared to find the optimal way for the preparation of the sintered body. The experimental results showed that using PEG400 as a liquid desiccant results in a lower deformation of the body compared to the natural drying process. Compared with vacuum debinding or air debinding, a two-step debinding process, which consisted of both a vacuum pyrolysis step and the following air debinding, is allowed to control the pyrolysis rate while suppressing the formation of defects in the alumina body. After optimization of the postprocessing, the relative density of the sample as high as 99.3%, and the Vickers hardness ~17.5 GPa. These properties are similar to the properties of alumina bodies prepared via the conventional shaping method.



## 1. Introduction

Additive manufacturing (AM), also referred to as three-dimensional (3D) Printing, describes a class of technologies in which a part is directly produced according to a digital model by gradually printing two-dimensional (2D) layers of material to eventually form the part [1]. Today, AM technologies are the state of the art in the plastic processing and metalworking industry [2]. However, the general properties of polymers or metals are not sufficient for some applications, and there is a high demand for 3D ceramic structures for the fabrication of advanced devices that can be operated at high temperatures or in harsh, corrosive environments, as well as for applications requiring high tribological, mechanical, and chemical resistance [3].

Current approaches to realize the AM of ceramic materials can be divided into two categories, i.e., direct and indirect fabrication techniques. Direct techniques immediately yield the sintered ceramic parts but may have a large number of defects due to internal stresses induced by temperature gradients or the very rough surfaces. Indirect AM methods require a subsequent process to obtain the sintered ceramic objects. This includes all techniques where the shaping of the objects involves a combination of ceramic powder and an organic binder. So far, ceramics shaped by stereolithography (SL) have been applied, e.g., in the semiconductor industry and for the fabrication of microelectromechanical systems, investment casting molds, photonic crystals, dental resins and scaffolds for tissue regeneration [3–7].

Recent studies on the stereolithography of ceramic materials generally focused on improving the rheological and curing properties [8–13]. For instance, the cure depth has been modeled by employing a modified Beer–Lambert law, and fully dense ceramic stereolithography parts were obtained from a 40 vol% alumina suspension in a diacrylate system by Griffith and Halloran, who were the first to adopt stereolithography for ceramic freeform fabrication [8]. Since then, a number of novel stereolithography methods have been developed [2,14]. For instance, an alumina body with a relative density of 93.2% has been fabricated using a novel mask-image-projection-based (MIP) stereolithography method combined with tape-casting [14]. Dense alumina ceramics have also been fabricated via the lithography-based ceramic manufacturing (LCM) technology developed by the Lithoz GmbH [2]. However, for both the MIP-SL and the LCM approach, it is difficult to fabricate large-sized parts due to the limitations of the digital micro-mirror device (DMD). Furthermore, for stereolithography in general, post-processing techniques, such as drying and debinding, have rarely been addressed, although they are vital

* Corresponding authors.
*E-mail addresses:* 317127238@qq.com (W. Liu), swu@gdut.edu.cn (S. Wu).
[1] Both authors contributed equally to this work.

http://dx.doi.org/10.1016/j.ceramint.2016.04.050
0272-8842/

for the successful fabrication of ceramics via stereolithography based on the aqueous acrylamide system.

Alumina based ceramics have been widely used as cutting tools due to their excellent hardness and abrasive resistance, good chemical stability, and high-temperature performance. The typical mechanical properties is as follows: bending strength from 700 to 900 MPa, rockwell hardness from 92 to 95 HRA, and fracture toughness from 4.9 to 8.5 MPa $m^{1/2}$. Besides, Typical sintering methods for fabricating alumina cutting tools are pressureless sintering, hot pressing sintering, spark plasma sintering, and microwave sintering, etc. In this study, stereolithography was adopted to fabricate a defect-free alumina ceramic cutting tool by optimizing the drying and debinding processes. Regarding the drying process, a novel drying method based on immersing the compact body into a liquid desiccant is compared with the traditional natural drying method. Regarding the debinding process after drying, three different approaches – pyrolysis in air, pyrolysis in vacuum, and a two-step debinding profile consisting of a vacuum pyrolysis step followed by pyrolysis in air – were compared in order to find a balance between process efficiency and safety.

## 2. Material and methods

### 2.1. Preparation of the ceramic suspension

The ceramic suspension was prepared as follows: first, an aqueous acrylamide solution was prepared by mixing acrylamide with methylene-bis-acrylamide (MBAM) in a 19:1 ratio in 75 wt% water. Then, 30 vol% alumina powder (TAIMEI CHEMICALS, TM-DAR, $D_{50}$=200 nm) was added to the aqueous acrylamide solution after the dispersant was mixed into the solution. Afterwards, the ceramic suspension was ball-milled for 18 h. In this study, 0.4 wt% polyvinyl pyrrolidone K15 (PVP K15) was used as the dispersant. After the ball-milling process, the bubbles in the ceramic suspension were removed by stirring and vacuum pumping. Then, the photoinitiator 1173 was mixed into the ceramic suspensions to produce a UV-curable ceramic suspension. The photoinitiator mass fraction was selected to 1 wt% of the aqueous acrylamide solution.

### 2.2. Ceramic forming by stereolithography

The 3D model was created using the UG software. Then the Magics software was used to generate the supporting structure and to slice the parts. The final data was then imported into the stereolithography machine. The alumina green body was obtained by stereolithography using aforementioned the ceramic suspension. The schematic illustration of the stereolithography process is shown in Fig. 1.

Each single pattern layer was cured by the ultraviolet laser that selective scans on the ceramic suspension. After the first layer has been cured, the supporting platform was moved down, and the ceramic suspension was recoated on the cured surface with a blade. Then, the second layer was cured using the same process. These steps were repeated until the whole green body of the alumina cutting tool was fabricated.

### 2.3. Post processing of the alumina green body

#### 2.3.1. Drying

After the green body is obtained, the residual water in the sample has to be removed by drying. A deformation of the sample can occur quite easily during the drying process. Hence, it is critical to control the drying process to protect the sample from deformation. A novel drying approach based on using PEG 400 as the liquid desiccant was adopted. The approach was compared with the traditional natural drying method. For the PEG-based extraction process, the sample was first immersed in PEG 400, which results in a uniform extraction rate in all directions. When applying the natural drying process, the sample was placed in air to allow the water to evaporate in a natural environment.

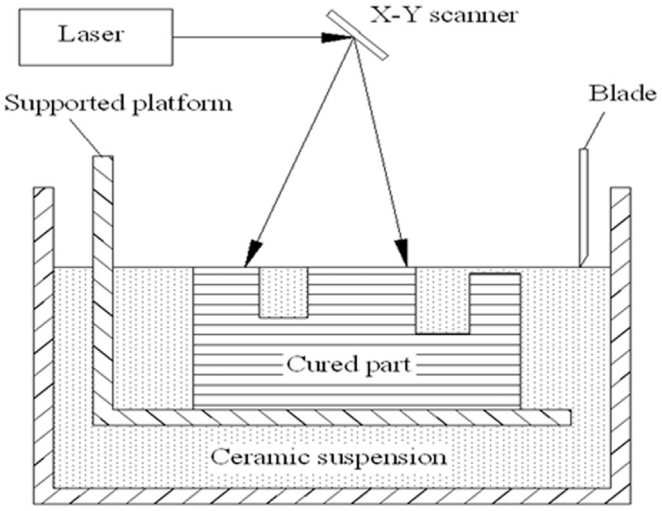


**Fig. 1.** The schematic illustration of the stereolithography process.

#### 2.3.2. Debinding

A suitable debinding process can prevent the sample from having defects. Three different debinding profiles were employed to find the optimal debinding process. The air pyrolysis debinding and the vacuum debinding profile are shown in Fig. 2(a), and the two-step debinding profile is shown in Fig. 2(b).

#### 2.3.3. Sintering

The samples were sintered in a furnace (Thermconcept, HTK 16/18, Germany) according to the sintering schedule as shown in Fig. 3.

### 2.4. Characterization

The density of the prepared alumina bodies was measured by applying the Archimedes' principle using a balance with an accuracy of 0.0001 g. The theoretical density of the alumina used in this study is 3.96 g/$cm^3$ according to the information provided by TAIMEI CHEMICALS. The Vickers-hardness was tested using a Vickers hardness testing machine (HVS-30Z, Shanghai Precision Instrument Co., Ltd., China) by applying a load of 49N. The microstructure of the sintered sample was characterized by scanning electron microscopy (SEM, Nova NanoSEM 430, FEI, Holland).

## 3. Results and discussion

### 3.1. Influence of the drying method on the shape and density of the alumina object

To investigate the effect of the drying process on the shape and density of the fabricated alumina body, the green bodies were dried via a natural drying process and a liquid desiccant (PEG)-assisted drying process, respectively. As shown in Fig. 4(a) and (b), an obvious deformation of the body occurred if the sample was allowed to dry naturally. This is attributed to the anisotropy of the water evaporation rate, which results from the inhomogeneity of the air flow on the different surfaces (Fig. 5(a)). In contrast, the

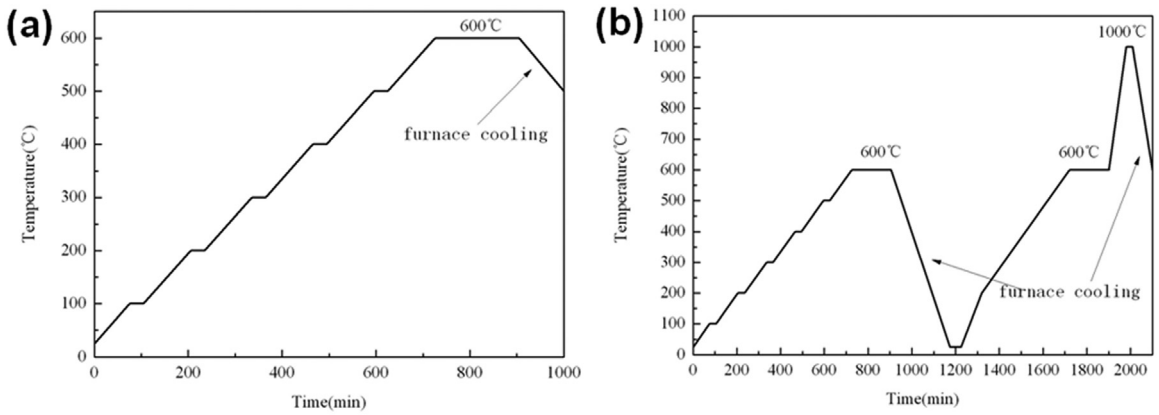


**Fig. 2.** (a) The air pyrolysis debinding and the vacuum debinding profile and (b) the two-step debinding profile.

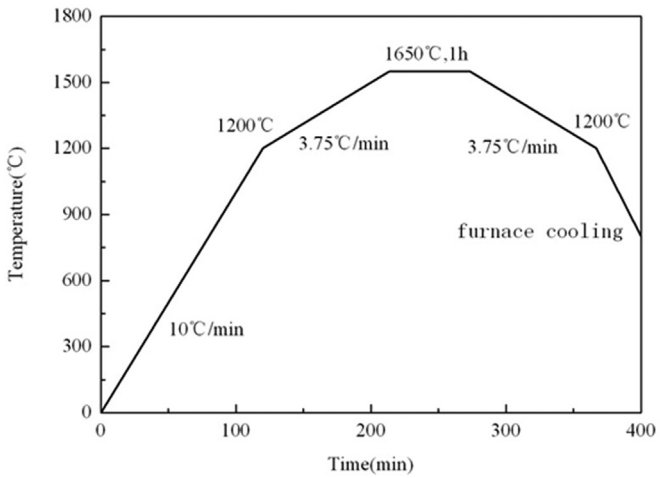


**Fig. 3.** The sintering schedule of the samples.

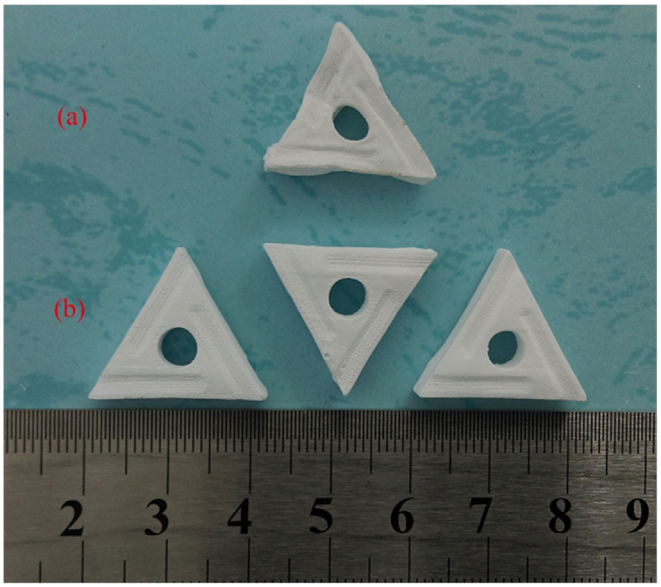


**Fig. 4.** (a) The green body dried via a natural drying process and (b) the green body dried via a liquid desiccant (PEG)-assisted drying process.

application of the liquid desiccant results in a more uniform water extraction rate, which leads to a much more homogeneous shrinkage, as shown in Fig. 5(c) and (d).

Except for the shape of the green body, it is also interesting to compare the relative density of the bodies obtained through the two different drying approaches. The relative density of the sample dried via the PEG-based approach is 99.3%, while the relative density of the sample dried in air is 96.2%. The reason for this difference is as follows: during the natural drying process, the surface of the sample always dried and shrunk first, which prevented the water inside the body from escaping, as shown in Fig. 5 (b). The pores generated by the trapped water during sintering would then lower the density of the resulting product.

### 3.2. *Influence of the debinding process on the defect density*

Three different debinding profiles were applied and compared in this study: air debinding, vacuum debinding and a two-step profile debinding. The sample that is debound in air exhibits a large number of defects, as shown in Fig. 6, which is attributed to the very high pyrolysis rate of the organic compound. The gas generated during the pyrolysis cannot escape from the body in time. Thus, a partial pressure is generated inside the body, resulting in the formation of defects.

Next, vacuum debinding was employed to control the pyrolysis rate, because the pyrolysis rate is much lower in a vacuum environment. The gas generated during the vacuum pyrolysis process can escape more easily from the channels between the particles in the body. However, the residual carbon in the debound body would produce gas during the following sintering process, leading to the formation of cracks in the body during sintering, as shown in Fig. 7(b).

Therefore, a two-step debinding process was adopted to protect the sample from having any defects. The first step of the debinding process was the aforementioned vacuum debinding. Then, as a second step, an air debinding process was applied, as shown in Fig. 2(b). The second step allows the elimination of the residual carbon before sintering, consequently preventing the generation of cracks can be prevented. The above debinding mechanism is similar to the two step debinding method which is solvent debinding followed by rapid thermal debinding in injection molding. For this debinding approach in ceramic injection molding, soluble binder is firstly removed while the interconnected pore channels are formed from exterior to interior, leaving the insoluble binders in the contact region, and the pore channels could serve as escape paths for decomposed gas during subsequent thermal debinding for insoluble binders. The binder system for solvent debinding

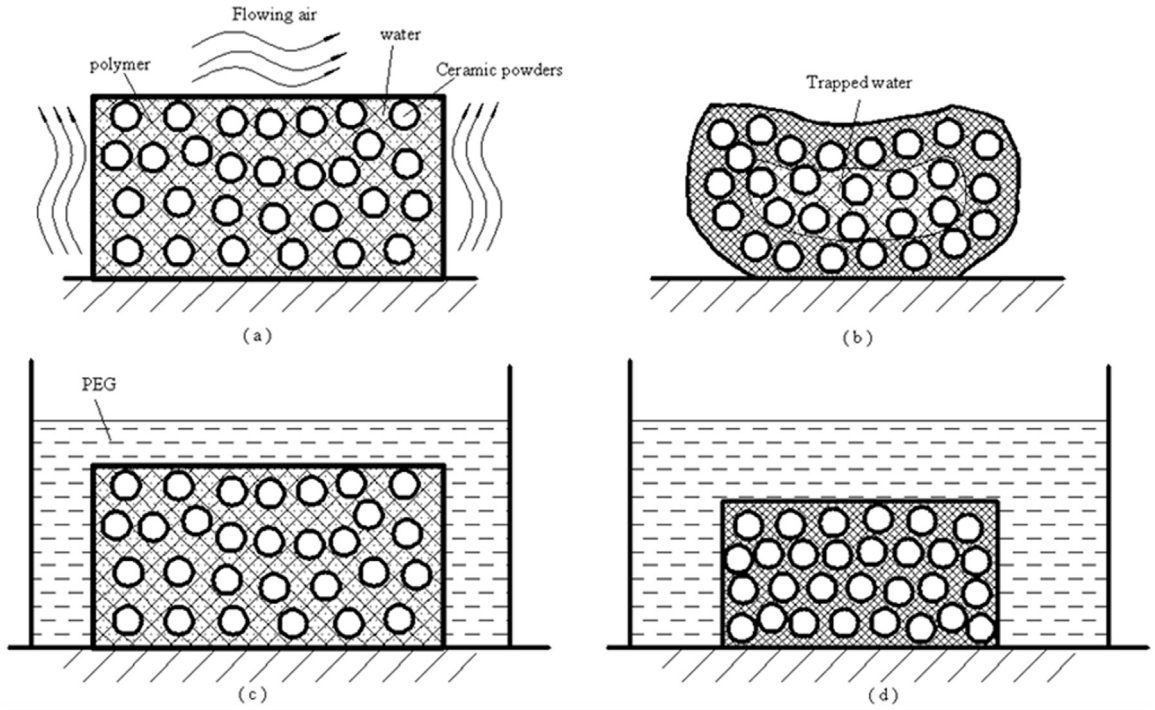


**Fig. 5.** The drying schematic program of (a, b) the natural drying sample and (c, d) the PEG-assisted drying sample.

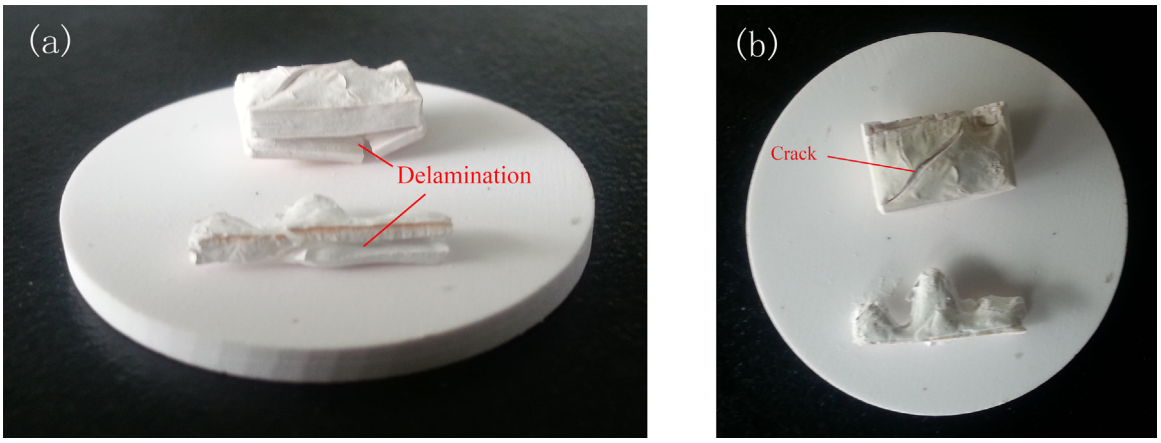


**Fig. 6.** The compact sample debound in air.

mainly consists of solvent soluble components, which dissolve in solvent and insoluble backbone binder which keeps the strength of the green body in the whole debinding process. Therefore, binder removal of solvent-based binder system is much easier than that of wax-based one since the pore channels originated from solvent-based binder could serve as escape paths for the following thermal pyrolysis as indicated above [15].

The sample obtained after the two-step profile sintering is shown in Fig. 7(a). There is no visible deformation, and the relative density was as high as 99.3%. The microstructure of the polished surface of the body sintered at 1650 °C is shown in Fig. 8. A relatively dense microstructure with only a small number of pores was obtained by combining the liquid desiccant-assisted drying with the two-step debinding process. The Vickers hardness of the obtained alumina cutting tool was determined to be ~17.5 Gpa. A systematic comparasion of the hardness in the present study with other forming and sintering conditions is shown in Table 1.

## 4. Conclusions

The liquid desiccant-based drying process is an efficient way to decrease the deformation of the green body during drying and improve the density, whereas a two-step profile debinding process is helpful to ensure the integrity of the sample. A dense defect-free alumina cutting tool with a relative density of 99.3% was fabricated via stereolithography followed by a combination of liquid desiccant drying and a two-step debinding process. The Vickers hardness of the sintered body was determined to be ~17.5 GPa, which is similar to the hardness of alumina prepared via the conventional shaping method.

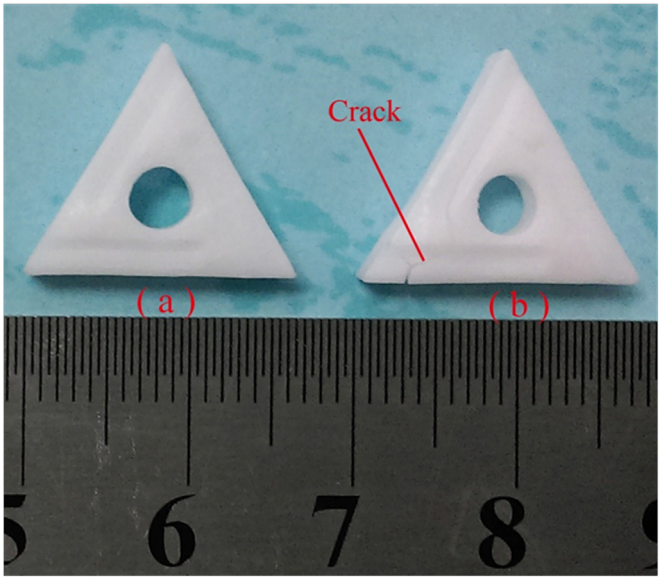


**Fig. 7.** The sintered body obtained from (a) a two-step profile debinding; (b) vacumm debinding.

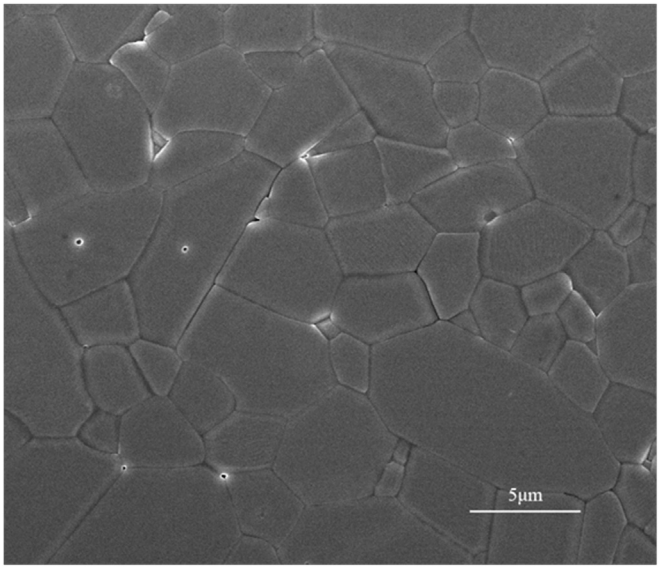


**Fig. 8.** The microstructure of the polished surface of the sintered body at 1650 °C via the combination of liquid desiccant drying and a two-step debinding profile.

**Table 1**
A systematic comparasion of hardness via 3D printing with other forming and sintering conditions.

| Reference | Forming method | Sintering process | Hardness (GPa) |
|---|---|---|---|
| Homemade | Automatic press and CIP | 1450 °C, 1 h, air | ~17.8 |
| [16] | Gel-casting | 1800 °C, air | 10.66 |
| [17] | Injection molding | 1425 °C, 2 h, $H_2$ | 20.87 |
| [18] | Tape casting | 1680 °C,1 h and 1600 °C, 2 h, air | 15.91 |
| [19] | Slip casting | 1700 °C, 2 h, Ar | 15.1 |
| [20] | Uniaxially pressed | Pressureless in air and then HIP in Ar | > 18 |

## Acknowledgment

This work was supported by Research Funding for Introduction of Guangdong Province Leading Talents (Grant no. 40012001), Project on the Integration of Industry, Education and Research of Guangdong Province (Grant no. 2011A090200080).

## References

[1] A. Zocca, P. Colombo, C.M. Gomes, J. Günster, Additive manufacturing of ceramics: issues, potentialities, and opportunities, J. Am. Ceram. Soc. 98 (2015) 1983–2001.
[2] M. Schwentenwein, J. Homa, Additive manufacturing of dense alumina ceramics, Int. J. Appl. Ceram. Technol. 12 (2015) 1–7.
[3] E. Zanchetta, M. Cattaldo, G. Franchin, M. Schwentenwein, J. Homa, G. Brusatin, P. Colombo, Stereolithography of SiOC ceramic microcomponents, Adv. Mater. (2015), http://dx.doi.org/10.1002/adma.201503470.
[4] D.I. Woodward, C.P. Purssell, D.R. Billson, D.A. Hutchins, S.J. Leigh, Additively-manufactured piezoelectric devices, Phys. Status Solidi A 212 (2015) 2107–2113.
[5] Q. Liang, D. Li, G. Yang, Rapid fabrication of diamond-structured ceramic photonic crystals with graded dielectric constant and its controllable stop band properties, Ceram. Int. 39 (2013) 153–157.
[6] W. Zhou, D. Li, Z. Chen, S. Chen, Direct fabrication of an integral ceramic mould by stereolithography, Proc. Inst. Mech. Eng. Part B: J. Eng. Manuf. 224 (2010) 237–243.
[7] F.P. Melchels, J. Feijen, D.W. Grijpma, A review on stereolithography and its applications in biomedical engineering, Biomaterials 31 (2010) 6121–6130.
[8] M.L. Griffith, J.W. Halloran, Freeform fabrication of ceramics via stereolithography, J. Am. Ceram. Soc. 79 (1996) 2601–2608.
[9] A. Goswami, Ankit K, N. Balashanmugam, A.M. Umarji, G. Madras, Optimization of rheological properties of photopolymerizable alumina suspensions for ceramic microstereolithography, Ceram. Int. 40 (2014) 3655–3665.
[10] S.P. Gentry, J.W. Halloran, Depth and width of cured lines in photopolymerizable ceramic suspensions, J. Eur. Ceram. Soc. 33 (2013) 1981–1988.
[11] T. Chartier, A. Badev, Y. Abouliatim, P. Lebaudy, L. Lecamp, Stereolithography process: influence of the rheology of silica suspensions and of the medium on polymerization kinetics – cured depth and width, J. Eur. Ceram. Soc. 32 (2012) 1625–1634.
[12] M. Wozniak, Y. de Hazan, T. Graule, D. Kata, Rheology of UV curable colloidal silica dispersions for rapid prototyping applications, J. Eur. Ceram. Soc. 31 (2011) 2221–2229.
[13] V. Tomeckova, J.W. Halloran, Critical energy for photopolymerization of ceramic suspensions in acrylate monomers, J. Eur. Ceram. Soc. 30 (2010) 3273–3282.
[14] X. Song, Y. Chen, T.W. Lee, S. Wu, L. Cheng, Ceramic fabrication using Mask-Image-Projection-based Stereolithography integrated with tape-casting, J. Manuf. Process. (2015), http://dx.doi.org/10.1016/j.jmapro.2015.06.022.
[15] W. Liu, X.F. Yang, Z.P. Xie, Cui Jia, L.L. Wang, Novel fabrication of injection-moulded ceramic parts with large section via partially water-debinding method, J. Eur. Ceram. Soc. 32 (2012) 2187–2191.
[16] M. Cao, Q. Yan, X. Li, Y. Mi, Effect of plate-like alumina on the properties of alumina ceramics prepared by gel-casting, Mater. Sci. Eng.: A 589 (2014) 97–100.
[17] F. Sommer, F. Kern, R. Gadow, Injection molding of ceramic cutting tools for wood-based materials, J. Eur. Ceram. Soc. 33 (2013) 3115–3122.
[18] M. Yu, J. Zhang, X. Li, H. Liang, H. Zhong, Y. Li, Y. Duan, D.L. Jiang, X. Liu, Z. Huang, Optimization of the tape casting process for development of high performance alumina ceramics, Ceram. Int. 41 (2015) 14845–14853.
[19] H. Reveron, O. Zaafrani, G. Fantozzi, Microstructure development, hardness, toughness and creep behaviour of pressureless sintered alumina/SiC micro–nanocomposites obtained by slip-casting, J. Eur. Ceram. Soc. 30 (2010) 1351–1357.
[20] M.H. Bocanegra-Bernal, C. Domínguez-Rios, A. Garcia-Reyes, A. Aguilar-Elguezabal, J. Echeberria, A. Nevarez-Rascon, Hot isostatic pressing (HIP) of α-$Al_2O_3$ submicron ceramics pressureless sintered at different temperatures: improvement in mechanical properties for use in total hip arthroplasty (THA), Int. J. Refract. Met. Hard Mater. 27 (2009) 900–906.